Effects of organic matter–goethite interactions on reactive transport of nalidixic acid: column study and modeling

Wei Cheng, Lian Zhou, Remi Marsac, Jean-François Boily, Khalil Hanna

Effects of organic matter–goethite interactions on reactive transport of nalidixic acid: column study and modeling

Wei Cheng, Lian Zhou, Rémi Marsac, Jean-François Boily, Khalil Hanna

PII: S0013-9351(20)31084-7

DOI: https://doi.org/10.1016/j.envres.2020.110187

Reference: YENRS 110187

To appear in: *Environmental Research*

Received Date: 25 May 2020

Revised Date: 25 August 2020

Accepted Date: 7 September 2020

Please cite this article as: Cheng, W., Zhou, L., Marsac, R., Boily, J.-F., Hanna, K., Effects of organic matter–goethite interactions on reactive transport of nalidixic acid: column study and modeling, *Environmental Research*, https://doi.org/10.1016/j.envres.2020.110187.

Effects of organic matter–goethite interactions on reactive transport of nalidixic acid: column study and modeling

Wei Cheng,[a,b] Lian Zhou,[b] Rémi Marsac,[c] Jean-François Boily[d] and Khalil Hanna[*b,e]

[a] *College of Resources and Environmental Science, South-Central University for Nationalities, Wuhan, China.*

[b] *Univ Rennes, École Nationale Supérieure de Chimie de Rennes, CNRS, ISCR – UMR6226, F-35000 Rennes, France*

[c] *Univ Rennes, CNRS, Géosciences Rennes - UMR 6118, F-35000 Rennes, France*

[d] *Department of Chemistry, Umeå University, SE-901 87 Umeå, Sweden*

[e] *Institut Universitaire de France (IUF), MESRI, 1 rue Descartes, 75231 Paris, France.*

*Corresponding author: Tel.: +33 2 23 23 80 27; Fax : +33 2 23 23 81 20

E-mail address: khalil.hanna@ensc-rennes.fr (K. Hanna)

A revised manuscript submitted to *Environmental Research*

August 2020

Graphical Abstract

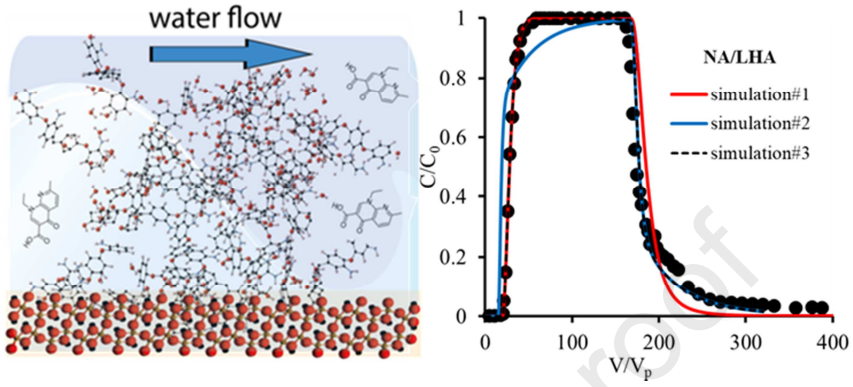

Abstract

The fractionation of natural organic matter (NOM) and its impact on the binding of quinolones to mineral surfaces and transport behaviour under flow-through conditions have been scarcely investigated. In this study, the sorption and transport of a widely used quinolone antibiotic, Nalidixic acid (NA), were investigated in goethite-coated sand (GCS) columns over a wide concentration range (5 – 50 mg/L) of Leonardite humic acid (LHA), a representative NOM. Simultaneous injection of NA and LHA in GCS columns mutually alter transport of each other, *i.e.* NA mobility and LHA molecular fractionation. Preloading of GCS column with LHA dramatically facilitated the transport behaviour of NA, where nonspecific interactions with LHA-covered goethite surfaces controlled NA mobility. Simulations using a two-site nonequilibrium model showed that a modified sorption rate constant was required to accurately describe the breakthrough curves of NA under these conditions. This altered rate constant suggests that nonspecific interactions of NA on bound LHA may take place as an additional binding mechanism affecting adsorption kinetics. NOM fractionation alters sorption mechanisms and kinetics of quinolone antibiotics, which in turn affect their fractionation. These results may have important implications for an accurate assessment of the fate of these types of antibiotics in aquatic environments.

Keywords: Quinolones; Adsorption; Column; Reactive transport; Modeling.

1. Introduction

Quinolone antibiotics are broad-spectra antimicrobial agents that are widely used in human and veterinary medicine to treat and prevent infectious bacterial diseases (Oliphant and Green, 2002). Due to their extensive uses and incomplete metabolisms *in vivo*, they can be disseminated into terrestrial and aquatic environments at concentrations as high as several hundred ng per L (Fatta-Kassinos et al., 2011). Adsorption to immobile soil/sediment minerals and/or mobile colloids is one of the key processes governing the fate and mobility of quinolones in environment (Marsac et al., 2016; Xu et al., 2017a; Yu et al., 2019). This process is strongly related to the nature and relative abundance of mineral phases of common occurrence in the Earth's near-surface environment (Cornell and Schwertmann, 2003). Among these reactive mineral surfaces, goethite (α-FeOOH) is the most common and stable iron oxyhydroxide mineral with high specific surface area and high reactivity (Liu et al., 2014), and generally found as coatings on less reactive soil particles, such as silica sand (Stumm et al., 1992), in soils and sediments.

Quinolones binding on minerals can however be strongly influenced by Natural Organic Matter (NOM) (Gu and Karthikeyan, 2008; Yan et al., 2012; Peng et al., 2015; Martínez-Mejía et al., 2017; Qin et al., 2018; Cheng et al., 2018). Some studies have suggested that the presence of NOM can provide additional sorption sites for quinolones due to hydrophobic interactions, π-πinteractions, ligand exchange, and hydrogen bonding between NOM and quinolones, thus promoting the adsorption of quinolones (Peng et al., 2015; Martínez-Mejía et al., 2017; Qin et al., 2018). However, other studies have reported that NOM will suppress quinolones binding because of the competition for sorption sites on minerals (Cheng et al., 2018), or electrostatic repulsions between the coated

NOM and quinolones (Gu and Karthikeyan, 2008; Yan et al., 2012). Although NOM may interact strongly with both minerals (Vindedahl et al., 2016) and antibiotics (Aristilde and Sposito, 2013; Richter et al., 2009), little is known about these co-occurring molecular interactions in natural settings where water migrates through soils and sediments. This is complicated by the complex nature of NOM — which consists of a polydisperse mixture of organic molecules of varying molecular size and chemical composition — and by its molecular fractionation resulting from its association to mineral surfaces. Currently available studies on the subject (Cheng et al., 2018; Kulshrestha et al., 2004; Qin et al., 2018; Yan et al., 2012) were limited to batch experiments, and little is known about the influence of NOM on binding and transport of antibiotics under flow-through conditions. Accounting for dynamic flow on nonequilibrium sorption of quinolones is particularly relevant when multiple mechanisms (*e.g.* binding *vs* co-binding and NOM molecular fractionation) concurrently influence breakthrough.

In this study, we addressed these concerns by studying the mobility of Nalidixic acid (NA), a model quinolone antibiotic, over a wide concentration range (5 – 50 mg/L) of Leonardite humic acid (LHA), a representative hydrophilic NOM. The NOM concentration range was chosen in order to cover a wide variety of dissolved organic carbon found in shallow groundwater, soil pore waters and surface waters (Degueldre et al., 1996; McKnight et al., 1992). Transport was studied under water saturated flow conditions, which are chosen to emulate contaminant migration and transformation in natural environments such as aquifer and sediments. Columns were packed with goethite-coated sand, a structurally stable and hydraulically conductive porous medium, to mimic natural mineral assemblages (Hanna et al., 2014). Impacts of LHA on NA transport was investigated in two scenarios:

(i) NOM initially present in contaminated water and then interact with co-occurring compound to mineral surfaces or (ii) NOM found as organic coatings on the mineral surface as in natural sedimentary materials (McKnight et al., 1992). In both cases, molecular fractionation of LHA and NA breakthrough were monitored by High Performance Liquid Chromatography (HPLC), UltraViolet Visible (UV-Vis) spectrophotometry and Total Organic Carbon (TOC) analyses of column effluents. A transport model that accounts for adsorption kinetics was used to help us in understanding the modifications in adsorption and desorption fronts of the breakthrough behavior of NA over a wide range of conditions. Changes in sorption kinetics can result from modifications in binding mechanisms and thus explain how NA transportation is facilitated in the presence of LHA.

2. Materials and methods

2.1. Materials

All reagents except Leonardite humic acid were purchased from Sigma-Aldrich and were used without further purification. All solutions were prepared with ultrapure water. Leonardite Humic Acid Standard (1S104H) was purchased from the International Humic Substance Society. A LHA stock solution (2 g/L, 1276 mg C/L) was prepared by dissolving 2 g LHA in 100 mL of 1 M NaOH, then diluted to 1 L with ultrapure water. A 1 mM stock solution of Nalidixic acid (NA) (purity >99%) was prepared by dissolving 1 mmole NA in 20 mL of 1 M NaOH, then diluted to 1 L with ultrapure water.

2.2. Synthesis of goethite–coated sand (GCS)

Goethite was prepared as described in previous studies (Marsac et al.,2016; Hanna et al., 2014),

and coated onto cleaned Fontainebleau quartz sand (100-150 μm) as previously detailed (Scheidegger et al.,1993; Hanna et al., 2014). All sample preparation and characterization procedures are in the Supplementary Material. All synthetic solids were washed with doubly distilled deionized water to remove soluble Fe and electrolyte ions. The solids were then stored in an anaerobic N_2(g) chamber at ambient temperature.

Previous work (Hanna et al., 2010, 2014) from our group confirmed that the coating procedure did not alter goethite particles and no silicates were released from quartz sand. The goethite content deposited on the sand surface, measured by acid digestion analysis, was 0.99 g/100 g of sand.

2.3. Breakthrough Column Experiments

Breakthrough column experiments were conducted at constant flow rate and under water-saturated conditions. pH conditions (i.e. pH 5) were specifically selected to ensure stable goethite coatings on sand and high adsorption of NA and LHA on goethite. Briefly, 15 g of dry goethite coated sand was packed into a glass chromatographic column of 1.6 cm internal diameter to give a porous bed length of 4.7 cm. After packing to a uniform bulk density (1.59 ± 0.05g/cm^3), the column was wetted upward with a 0.01 M NaCl solution at pH_{in} 5 and 0.5 mL/min. The pore volume (V_P) was estimated by weight differences between the saturated and dry column. Once the column became water saturated, the flow characteristics of the porous bed were determined by a nonreactive tracer (bromide) experiment and described by the classic advection dispersion equation (ADE). The fitting parameters of the bromide elution confirmed the flow homogeneity and predominance of a convective regime in the column.

10 μM NA and different concentrations of LHA (0, 5, 10, 50 mg/L) were equilibrated in 0.01 M

NaCl at pH_{in} 5 and then injected simultaneously into column at 0.5 mL/min. LHA and NA concentrations in the effluents were measured. After total breakthrough of NA/LHA, desorption was initiated by injecting 0.01 M NaCl at pH_{in} 5 into column at 0.5 mL/min. After the desorption of NA/LHA, the solid was transferred to 0.1 M NaOH and shaken for 1 week. Then the supernatants were filtered (0.2 μm), and analyzed by UV-Vis spectrometry and TOC analyzer.

In another experimental series, a LHA solution (5, 10 or 50 mg/L) in 0.01 M NaCl at pH_{in} 5 was thereafter injected into the column with a continuous mode at 0.5 mL/min. The effluent of the column was collected and stored at 4°C for further analyses. After the complete breakthrough of LHA, 10 μM NA with the corresponding LHA (5, 10, 50 mg/L) in 0.01 M NaCl at pH_{in} 5 was injected in the same column at the same constant flow rate. NA concentrations in the collected fractions were measured by HPLC/UV.

The concentration of LHA in the effluent solution was determined by a total organic carbon (TOC) analyzer (Shimadzu TOC-VCSH). The UV absorbance of LHA samples were recorded in the range of 200 - 800 nm with a UV–visible spectrophotometer using 1 cm quartz cell. The following specific UV absorbance parameters were calculated as indicators of NOM fractionation. The relative absorbance ratio E_2/E_3 is defined as the ratio of absorbance at 250 nm and 365 nm. E_2/E_3 has been reported to inversely correlate with the molecular weight (Mw) and aromaticity of NOM (Li et al., 2009; Peuravuori and Pihlaja, 1997; Qin et al., 2015). Specific ultraviolet absorbance of LHA at 280 nm ($SUVA_{280}$) was used to estimate NOM aromaticity by dividing the molar absorptivity at 280 nm (m^{-1}) by the TOC concentration (mg/L) in the solution (Qin et al., 2015; Hur et al., 2003). The parameter S_R (slope ratio) is the ratio of the slope of the shorter wavelength region (275 nm – 295 nm)

153 to that of the longer wavelength region (350 nm – 400 nm) (Helms et al., 2008). S_R is reported to be
154 negatively correlated with the Mw (Helms et al., 2008; Valencia et al., 2013).

155 Aqueous NA concentrations were determined by high performance liquid chromatography
156 (Waters 600 Controller) using a UV detector (Waters 2489) and a reversed-phase C18 column (250
157 mm×4.6 mm i.d., 5 μm). The mobile phase (1 mL/min) was a mixture of acetonitrile/water (60:40 v/v)
158 contained 0.1% formic acid. The detector was set to 258 nm for NA.

159 Column experiments were conducted in duplicates and showed a good reproducibility within 5 %
160 of relative standard deviation.

161 *2.4. Model approach*

162 The transport of NA both in the presence and absence of LHA through the columns was simulated
163 using a one-dimensional advection-dispersion model coupled with two-site nonequilibrium
164 adsorption model (van Genuchten and Wagenet, 1989). The two-site nonequilibrium model is based
165 on the assumption that two types of sorption sites exist, an equilibrium site and a kinetic site.
166 Sorption is instantaneous on the equilibrium site and described by a sorption isotherm (Type 1,
167 equilibrium), and time dependent on the kinetics site and follows first-order kinetics (Type 2, kinetic)
168 (van Genuchten and Wagenet, 1989). The final governing equations of the model are given by:

169 $$\frac{\partial C}{\partial t} + \left(\frac{\rho}{\theta}\right)\left(\frac{\partial S_1}{\partial t} + \frac{\partial S_2}{\partial t}\right) = D\frac{\partial^2 C}{\partial x^2} - v\frac{\partial C}{\partial x} \quad (1)$$

170 $$S_1 = K_d C^{\beta} \quad (2)$$

171 $$\frac{\partial S_2}{\partial t} = \alpha\left[(1-f)K_d C^{\beta} - S_2\right] \quad (3)$$

172 In these equations, C is the volume-averaged solution concentration of the adsorbate (NA) (μM), t is
173 time (h), ρ is the bulk density of goethite-coated sand in the column (g/cm^3), θ is the volumetric water

content (cm^3/cm^3), and it equals to the porosity of the saturated column, S_1 and S_2 are sorbed-phase concentrations of NA on the equilibrium and kinetic nonequilibrium sites (μmol/g), respectively, D is the dispersion coefficient (cm^2/h), x is distance (cm), v is the average pore water velocity (cm/h), f is the fraction of equilibrium sites (Type 1), α is the first-order rate coefficient associated with the kinetic site (h^{-1}), and K_d is the Freundlich isotherm adsorption coefficient (cm^3/g) related to the sorption capacity, and β is the Freundlich exponent that characterizes the degree of nonlinearity.

Hydrus-1D program was used to obtain the model parameters for the two-site nonequilibrium model. The values of θ and D were obtained by fitting the breakthrough data of the Br^- tracer, and the values of β, K_d, f and α were obtained by fitting the transport data of NA. The best fitted f value to describe the mobility of NA alone lied at 0.6. This value was then kept constant for all simulations, which allows to reduce the number of estimated parameters. A complete sensitivity analysis, including the modeling approach used in the present work, is provided in the Supplementary Material.

3. Results and discussion

3.1. Mutual effects of NA sorption and LHA molecular fractionation

Simultaneous injection of NA and LHA in goethite-coated sand column alters NA mobility. This can be seen through the increased steepness of asymmetrical breakthrough curve of NA at larger LHA concentrations while the breakthrough point remained constant (Fig. 1). The latter was shifted down only with the highest concentration of LHA (i.e. 50 mg/L), leading to a rapid breakthrough of NA. While the NA retention did not vary the outflow pH, probably due to the low NA loading (10 μM), the presence of LHA caused pH variations in the initial stage. The increase in pH suggested that proton

co-sorption is involved when the COO- groups of LHA replaced the surface –OH on goethite due to ligand exchange mechanism (Gu et al., 1994). At higher LHA loading, more COO- groups replaced surface –OH group resulting in more significant increase in pH. When all –OH groups are consumed, the effluent pH decreased and finally approached the influent pH after reaching total breakthrough (Fig. 1).

Since both NA and LHA can bind to goethite through ligand-exchange and hydrogen bonding (Cheng et al., 2019; Xu et al., 2017a), competing for surface sorption sites could occur during simultaneous injection. Oxygenated polycyclic aromatics and carboxylic compounds, which generally contain in DOM of high oxidation state and high aromaticity, tend to have higher affinities for iron oxyhydroxides than alcohols, ethers and aliphatics (Cheng et al., 2019; Lv et al., 2016, 2018; Coward et al., 2019). As LHA exhibits high chemical heterogeneity with higher aromaticity (i.e. carbon aromaticity of 0.58) (Thorn and Cox, 2009) and lower aliphatic carbons contents, we expect a molecular fractionation caused by selective adsorption of LHA to goethite (Coward et al., 2019; Kleber et al., 2007). This falls in line with the breakthrough behavior of LHA in goethite-coated sand column, particularly in terms of the discrepancy between TOC and UV (Fig. 2 for LHA without NA).

Higher TOC values with respect to UV absorbance at 254 nm were observed during the first adsorption stage, before both of the two parameters followed each other to reach their inflow values. This can also be seen by the low $SUVA_{280}$ values observed at the first stage (lower PV values), suggesting that aromatics were primarily and preferentially adsorbed to goethite in the column. In addition, E_2/E_3 (Abs_{250nm}/Abs_{365nm}) and S_R of outflow solution were first lower than the initial value of

LHA and then increased sharply, and finally decreased to reach the initial value (Fig. 2c,d). This confirms that LHA compounds with smaller molecular size were preferentially retained, leading to higher Mw fractions in the column effluent (lower E_2/E_3 and S_R than the initial LHA). The increase in both parameters above the initial value suggested that outflow solution contained lower Mw fractions with higher aromaticity, while higher Mw fractions were adsorbed in the column. Note that different reports have contrast results for humic acids fractionation onto Fe-oxides, which is likely related to the HA nature/source (Kang and Xing, 2008; Qin et al., 2015, 2012; Seders Dietrich et al., 2013; Zhou et al., 2001). Higher molecular weight were preferentially adsorbed and then replaced by lower ones in solution for commercial HA (Sinopharm Chemical Reagent Co. Ltd. China.) to goethite (Qin et al., 2015), while in other reports lower Mw molecules of NOM are firstly adsorbed onto iron oxides and successively replaced by higher Mw fractions (Kang and Xing, 2008; Qin et al., 2012; Seders Dietrich et al., 2013; Zhou et al., 2001). The preferential adsorption of relatively small size fractions can be explained by their fast diffusion to the mineral surface, while the bigger HA compounds containing more reactive groups can exhibit stronger overall binding, and thus replace the lower Mw fractions during the adsorption process (Weng et al., 2007). The primary adsorption of lower Mw of LHA aromatic components were also confirmed under batch conditions, where fast and simultaneous decrease in TOC and UV was observed over the first 15 min of contact time (Fig. S1a). Higher TOC values relative to UV were observed during adsorption kinetics, while E_2/E_3 and S_R values tend to exceed the initial value after 6 h of contact time (Fig. S1b), suggesting that the lower Mw of LHA components first adsorbed may be replaced by the larger LHA components on the goethite surface. This is consistent with a recent kinetic study (Coward et al., 2019) showing a rapid primary phase

adsorption of aromatic and polycyclic aromatic compounds to goethite at the first stage, followed by lignin-like and aliphatic compounds.

On the other hand, LHA fractionation under simultaneous injection with NA is illustrated using the relative UV absorbance at 254 nm (ΔA_{250}) and 400 nm (ΔA_{400}) of outflow solutions for the three LHA concentrations (empty symbols in Fig. 3). Except at the highest LHA loading (50 mg/L), the breakthrough curves display a first step where high absorbance values were observed following by a classical breakthrough step, whereby ΔA_{400} gradually increased from zero and tended to 1 (complete breakthrough). The beginning of a second step coincides with the NA breakthrough, suggesting that NA adsorption at the first step may influence LHA retention and thus mobilize some LHA compounds. Compounds that are flushed out early have greater A_{400}/A_{254} ratios than in raw LHA (Fig. 3 and Fig. S2). The greater absorbance at 400 nm is attributed to π - π^* transitions of polycyclic aromatic compounds (Chen et al., 2002). This suggests that the smaller aromatic compounds are preferentially adsorbed than multiple benzene ring structures at the first stage of breakthrough. This result is also consistent with the fractionation of LHA in column where lower Mw fractions were preferentially adsorbed (lower E_2/E_3 and S_R than the initial LHA in Fig. 2).

It is worth noting that this early breakthrough of aromatics is not observed in LHA transport experiments in the absence of NA (See UV absorbance at 400 nm in Fig. S3), confirming the impact of NA retention on the LHA molecular fractionation in column. NA likely increased the mobility of some LHA compounds through competitive binding with goethite surfaces. The full breakthrough behavior of LHA in goethite-coated sand columns was also found affected by the co-existing NA (See Breakthrough Curve (BTC) of LHA with and without NA in Fig. S4).

258

259 At low LHA loadings (5 or 10 mg/L), both NA and LHA compounds bind to surface sites of goethite
260 and the breakthrough of NA was only altered in the adsorption front (Fig. 1). In contrast, at higher
261 LHA loading (50 mg/L), NA breakthrough was altered both in the initial breakthrough point and
262 adsorption front. This rapid breakthrough of NA is likely ascribed to strong competitive adsorption of
263 LHA compounds to goethite, as well as intermolecular interactions between NA and unbound LHA
264 that decreased NA retention. This was confirmed further by a fluorescence test shown in Fig. S6.
265 This breakthrough behavior can be understood in terms of the competitive binding of NA and
266 carboxylic/aromatics compounds of LHA to the same surface sites of goethite (Cheng et al., 2019; Gu
267 et al., 1994). In particular, ligand exchange reaction with singly-coordinate −OH sites of goethite
268 (Cheng et al., 2019) is likely to drive the first step in the breakthrough curve as our previous
269 spectroscopic work (Xu et al., 2017b) shows that NA binds both as metal- and hydrogen-bonded
270 complexes on these sites. Therefore, competitive binding of NA and carboxylic/aromatics compounds
271 of LHA on −OH sites occur at the first step, followed probably by further adsorption of NA to LHA
272 covered goethite. We note that low amount of reactive phase (i.e. goethite ~ 1wt %) in coated sand
273 material as well as the low amount of adsorbed NA (0.06-0.24 μmol / m^2) hinder our ability to directly
274 assess possible modifications in binding mechanisms in the column system. In addition, the great
275 molecular complexity of LHA components and the strong overlapping of vibrational bands of NA and
276 LHA compounds explain why our attempt to get molecular-level details in the ternary
277 NA/LHA/goethite system failed. Instead, we used a macroscopic sorption model as a mean to examine
278 the possibility of different mechanisms involved during the simultaneous injection of NA and LHA. In

279 particular, a model integrating a sorption kinetic term was applied as a theoretical tool to describe the
280 influence of LHA on NA adsorption behavior. The model adequately predicted NA adsorption ($r^2 \geq$
281 0.9823, Table 1) using a lower K_d but a higher α at high LHA concentrations, thus suggesting the
282 modification of sorption mechanisms. The lower K_d indicates smaller NA surface loadings, whereas
283 the total amount of NA adsorbed was positively correlated with K_d (Fig. S7). Moreover, the higher α
284 value indicates faster kinetics, as suggested by the less tailing of NA in the presence of LHA (Fig. 1).
285 The long tailing observed in the breakthrough curve of NA without LHA was likely caused by
286 chemical kinetic limitations, as previously reported (Hanna et al., 2012, 2010), and confirmed here for
287 NA by the tailing mitigation obtained when a lower flow rate (0.1 mL/min) was applied (See Fig. S8).
288 To test whether modification of sorption kinetics takes place when NA interacts with LHA-covered
289 goethite, injection of NA in LHA preloaded columns was investigated, as detailed in the following
290 section.

291 *3.2. Sorption of NA in LHA preloaded columns*

292 Preloading of goethite coated sand columns with LHA dramatically changed the transport
293 behavior of NA in terms of both retardation factor and breakthrough curve shape (Fig. 4).
294 Asymmetrical curve shape with an extensive tailing became sigmoidal when NA was injected in
295 LHA preloaded columns. Increasing in LHA concentrations (from 0 to 50 mg/L) advanced the
296 breakthrough point, yet the latter remained very close for the three tested LHA concentrations.
297 Overall, the preliminary loading of column with LHA considerably facilitated the transport of NA,
298 with a very similar breakthrough behavior over the concentration range of LHA (5-50 mg/L).

299 As LHA ligand exchange predominantly involves ~3.3 sites/nm^2 of the reactive

300 singly-coordinated −OH groups of goethite (Cheng et al., 2019), it becomes useful to express
301 breakthrough results in terms of surface loadings. Based on our previous work (Cheng et al., 2019),
302 goethite surfaces expose a mixture of non-reacted −OH groups and bound LHA at C/Fe ratios below
303 0.1 (namely, 26 C/nm^2). All -OH groups are, on the other hand, consumed above this ratio (Cheng et
304 al., 2019). Using the TOC of column effluents (Fig. 2a), the integrated area above the BTC shows
305 that the total LHA adsorbed in the column was ~75 mg C/g goethite, which is equivalent to ~42 C
306 atoms/nm^2 and therefore ~3 times the total crystallographic density of all surface oxygens (~15
307 sites/nm^2) (Boily and Felmy, 2008; Cheng et al., 2019).

308 Under these conditions, NA retention was mainly driven by weak van der Waals-type hydrophobic
309 interactions, and/or through π–π electron coupling interactions with LHA-covered goethite surfaces.
310 These interactions could govern the transport behavior in preloaded columns, independently on the
311 LHA preloading concentration. This hypothesis was further confirmed in the simulation results using
312 a two-site nonequilibrium model of the breakthrough curves of NA in LHA-preloaded columns.
313 Similar adsorption parameters (K_d, α and β) described the breakthrough curve of NA for the three
314 preloading LHA concentration (Fig. 4, Table 1). The first-order rate coefficient associated with the
315 kinetically limited site (α) increased when column is previously loaded with LHA, suggesting the
316 modification of NA sorption kinetics. This phenomenon is also observed under batch conditions where
317 the presence of LHA affected the adsorption kinetics of NA (Fig. S10).

318 *3.3. Impact of LHA on the breakthrough behavior of NA*

319 Dynamic adsorption experiments in column provided relevant data on the dual binding
320 mechanisms of NA, *i.e.* adsorption to (i) goethite in competition with carboxylic/aromatics LHA

compounds, and (ii) LHA-covered goethite through nonspecific interactions, together with the molecular fractionation of LHA. To highlight the impact of LHA on the NA mobility/transport in the column system, full breakthrough curve consisting of both adsorption/desorption fronts was determined for NA alone and NA in presence of 50 mg/L LHA.

As shown in Fig. 5a, the full breakthrough curve of NA is asymmetrical, and exhibits tailing both in adsorption front and elution-wave, confirming the rate-limited sorption/desorption process of NA on goethite surfaces. Interestingly, the desorption front can be well predicted with the same parameters used for the adsorption, suggesting a reversible sorption process. As expected from previous column tests, the presence of LHA alters the desorption front, making the full breakthrough curve of NA more symmetrical, with less tailing in both adsorption and desorption fronts (Fig. 5b and Fig. S11). As it is difficult to directly access molecular-level information in the NA/LHA/goethite system, we have used the same model as for the previous column adsorption experiments, to describe the influence of LHA on NA mobility. If the same adsorption parameters (i.e. α, K_d, β) were used for full BTC description, the calculated curve failed to well describe the desorption tailing (Simulation#1 in Fig. 5b). Attempt to describe better the latter by changing α (see Table S1) provided a curve where adsorption front is shifted down with respect to the experimental data (Simulation#2). An accurate description of the full breakthrough curve required two different values of α for adsorption and desorption fronts (Simulation#3, See Table S1). Indeed, lower α for desorption than adsorption was needed, thereby underscoring possible modification of surface reactions. Due to the very slow and incomplete desorption of LHA compounds in column, the amount of LHA desorbed in the effluent solution becomes below detection limit after 5 PV (Fig. S12), and extension up to 800 PV had no influence on

342 the amount of LHA desorbed (data not shown). Solid-phase extraction conducted on the goethite
343 coated sand solid after termination of the column experiment revealed that at least 80 % of total sorbed
344 LHA are still present on the solid (total LHA adsorbed in the column was ~75 mg C/g goethite or
345 ~42 C atoms/nm^2). This can also be observed visually since the solid kept its brown color (due to the
346 attachment of LHA), confirming the incomplete LHA desorption under our experimental conditions
347 and over the whole breakthrough time. A desorption batch experiment showed that only 40 % of initial
348 bound LHA (based on TOC measurement) were removed after 3 days and even under vigorous mixing
349 conditions (Fig. S13). This is consistent with previous works (Gu et al., 1994; Joo et al., 2008) where
350 the slow desorption kinetics and low desorption extent of NOM at oxide surfaces have been
351 attributed to the complex nature of NOM compounds (though different NOM were used in these
352 studies) and their multiple interactions involving multiple binding sites with oxide surfaces (Gu et al.,
353 1994; Joo et al., 2008). Therefore, experimental observations and simulation results suggested that
354 nonspecific interactions between NA and bound LHA compounds may influence desorption process.
355 While NA desorption is almost complete, most of sorbed LHA compounds remained attached to
356 goethite surfaces, resulting in modification in desorption kinetics.
357

358 **4. Conclusions**

359 NOM, one of the most widespread and ubiquitous components in aquatic and terrestrial
360 environments, can affect the mobility and fate of emerging contaminants. Here, we have considered
361 two situations where target contaminants (i) are present together with NOM in groundwater and
362 surface waters, then bind to mineral surfaces, and (ii) where they interact with NOM coatings on

363 minerals. In both scenarios, NOM strongly affected quinolone binding to goethite, and thus transport
364 behavior under flow through conditions. We notably demonstrated that LHA facilitated NA transport
365 in columns but this effect depends on how organic matter is contacted to mineral surfaces. When
366 LHA was present as a mineral coating, van der Waals-type hydrophobic interactions governed NA
367 transport. However, when both LHA and NA were initially present in the influent solution, the
368 breakthrough was characterized first by a primary step involving competitive adsorption of NA and
369 carboxylic/aromatics compounds, and a second step involving nonspecific adsorption of NA to
370 LHA-covered goethite. This two-step process controls both NA retention and LHA molecular
371 fractionation in column. NOM fractionation alters sorption mechanisms and kinetics of quinolone
372 antibiotics, which in turn affect their fractionation. Furthermore, the low and incomplete desorption
373 of LHA compounds from mineral surfaces also alters the desorption and mobility of NA under flow
374 through conditions.

375 Our work thereby shows how molecular interactions between the NOM and soil materials control
376 the migration of contaminants within surface and subsurface environments. This calls for in-depth
377 consideration of molecular characteristics of binding mechanisms in assessment studies of
378 contaminant fate. These findings can have important implications on the prediction of transport of
379 quinolone antibiotics, and of their ecological impacts in the environment.

380

381 **Acknowledgements**

382 This work was supported by the Centre National de la Recherche Scientifique (PICS CNRS
383 2018-2020), the Swedish Research Council (2016-03808), and the French National Research Agency

via the C-FACTOR project (ANR-18-CE01-0008-01).

Supplementary Material

Details of the synthesis and characterization of goethite and goethite coated sand; kinetics experiment conditions and results; experimental and calculated breakthrough curves; UV spectra; Fluorescence results; Sensitivity tests.

390 **References**

391 Aristilde, L., Sposito, G., 2013. Complexes of the antimicrobial ciprofloxacin with soil, peat, and
392 aquatic humic substances. Environ. Toxicol. Chem. 32, 1467–1478.
393 https://doi.org/10.1002/etc.2214.

394 Boily, J.-F., Felmy, A.R., 2008. On the protonation of oxo- and hydroxo-groups of the goethite
395 (α-FeOOH) surface: A FTIR spectroscopic investigation of surface O–H stretching vibrations.
396 Geochim. Cosmochim. Acta 72, 3338–3357. https://doi.org/10.1016/j.gca.2008.04.022.

397 Chen, J., Gu, B., LeBoeuf, E.J., Pan, H., Dai, S., 2002. Spectroscopic characterization of the structural
398 and functional properties of natural organic matter fractions. Chemosphere 48, 59–68.
399 https://doi.org/10.1016/S0045-6535(02)00041-3.

400 Cheng, W., Hanna, K., Boily, J.-F., 2019. Water Vapor Binding on Organic Matter-Coated Minerals.
401 Environ. Sci. Technol. https://doi.org/10.1021/acs.est.8b05134.

402 Cheng, W., Marsac, R., Hanna, K., 2018. Influence of Magnetite Stoichiometry on the Binding of
403 Emerging Organic Contaminants. Environ. Sci. Technol. 52, 467–473.
404 https://doi.org/10.1021/acs.est.7b04849.

405 Cornell, R.M., Schwertmann, U., 2003. The iron oxides structure, properties, reactions, occurences
406 and uses. Wiley-VCH, Weinheim; Cambridge.

407 Coward, E.K., Ohno, T., Sparks, D.L., 2019. Direct Evidence for Temporal Molecular Fractionation of
408 Dissolved Organic Matter at the Iron Oxyhydroxide Interface. Environ. Sci. Technol. 53, 642–650.
409 https://doi.org/10.1021/acs.est.8b04687.

410 Degueldre, C., Pfeiffer, H.-R., Alexander, W., Wernli, B., Bruetsch, R., 1996. Colloid properties in

411 granitic groundwater systems. I: Sampling and characterisation. Appl. Geochem. 11, 677–695.
412 https://doi.org/10.1016/S0883-2927(96)00036-4.
413 Fatta-Kassinos, D., Meric, S., Nikolaou, A., 2011. Pharmaceutical residues in environmental waters
414 and wastewater: current state of knowledge and future research. Anal. Bioanal. Chem. 399, 251–
415 275. https://doi.org/10.1007/s00216-010-4300-9.
416 Gaboriaud, F., Ehrhardt, J.-J., 2003. Effects of different crystal faces on the surface charge of colloidal
417 goethite (α-FeOOH) particles: an experimental and modeling study. Geochim. Cosmochim. Acta 67,
418 967–983. https://doi.org/10.1016/S0016-7037(02)00988-2.
419 Gu, Baohua., Schmitt, Juergen., Chen, Zhihong., Liang, Liyuan., McCarthy, J.F., 1994. Adsorption and
420 desorption of natural organic matter on iron oxide: mechanisms and models. Environ. Sci. Technol.
421 28, 38–46. https://doi.org/10.1021/es00050a007.
422 Gu, C., Karthikeyan, K.G., 2008. Sorption of the Antibiotic Tetracycline to Humic-Mineral
423 Complexes. J. Environ. Qual. 37, 704–711. https://doi.org/10.2134/jeq2007.0030.
424 Hanna, K., Boily, J.-F., 2010. Sorption of Two Naphthoic Acids to Goethite Surface under Flow
425 through Conditions. Environ. Sci. Technol. 44, 8863–8869. https://doi.org/10.1021/es102903n.
426 Hanna, K., Lassabatere, L., Bechet, B., 2012. Transport of two naphthoic acids and salicylic acid in
427 soil: experimental study and empirical modeling. Water Res. 46, 4457–4467.
428 https://doi.org/10.1016/j.watres.2012.04.037.
429 Hanna, K., Martin, S., Quilès, F., Boily, J.-F., 2014. Sorption of Phthalic Acid at Goethite Surfaces
430 under Flow-Through Conditions. Langmuir 30, 6800–6807. https://doi.org/10.1021/la4049715.
431 Hanna, K., Rusch, B., Lassabatere, L., Hofmann, A., Humbert, B., 2010. Reactive transport of gentisic

acid in a hematite-coated sand column: Experimental study and modeling. Geochim. Cosmochim. Acta 74, 3351–3366. https://doi.org/10.1016/j.gca.2010.03.022.

Helms, J.R., Stubbins, A., Ritchie, J.D., Minor, E.C., Kieber, D.J., Mopper, K., 2008. Absorption spectral slopes and slope ratios as indicators of molecular weight, source, and photobleaching of chromophoric dissolved organic matter. Limnol. Oceanogr. 53, 955–969. https://doi.org/10.4319/lo.2008.53.3.0955.

Hur, J., Schlautman, M.A., 2003. Using Selected Operational Descriptors to Examine the Heterogeneity within a Bulk Humic Substance. Environ. Sci. Technol. 37, 880–887. https://doi.org/10.1021/es0260824.

Joo, J.C., Shackelford, C.D., Reardon, K.F., 2008. Association of humic acid with metal (hydr)oxide-coated sands at solid–water interfaces. J. Colloid Interface Sci. 317, 424–433. https://doi.org/10.1016/j.jcis.2007.09.061.

Kang, S., Xing, B., 2008. Humic Acid Fractionation upon Sequential Adsorption onto Goethite. Langmuir 24, 2525–2531. https://doi.org/10.1021/la702914q.

Kleber, M., Sollins, P., Sutton, R., 2007. A conceptual model of organo-mineral interactions in soils: self-assembly of organic molecular fragments into zonal structures on mineral surfaces. Biogeochemistry 85, 9–24. https://doi.org/10.1007/s10533-007-9103-5.

Kulshrestha, P., Giese, R.F., Aga, D.S., 2004. Investigating the Molecular Interactions of Oxytetracycline in Clay and Organic Matter: Insights on Factors Affecting Its Mobility in Soil. Environ. Sci. Technol. 38, 4097–4105. https://doi.org/10.1021/es034856q.

Li, A., Hu, J., Li, W., Zhang, W., Wang, X., 2009. Polarity based fractionation of fulvic acids.

453 Chemosphere 77, 1419–1426. https://doi.org/10.1016/j.chemosphere.2009.09.002.
454 Liu, H., Chen, T., Frost, R.L., 2014. An overview of the role of goethite surfaces in the environment.
455 Chemosphere 103, 1–11. https://doi.org/10.1016/j.chemosphere.2013.11.065.
456 Lv, J., Miao, Y., Huang, Z., Han, R., Zhang, S., 2018. Facet-Mediated Adsorption and Molecular
457 Fractionation of Humic Substances on Hematite Surfaces. Environ. Sci. Technol. acs.est.8b03940.
458 https://doi.org/10.1021/acs.est.8b03940.
459 Lv, J., Zhang, S., Wang, S., Luo, L., Cao, D., Christie, P., 2016. Molecular-Scale Investigation with
460 ESI-FT-ICR-MS on Fractionation of Dissolved Organic Matter Induced by Adsorption on Iron
461 Oxyhydroxides. Environ. Sci. Technol. 50, 2328–2336. https://doi.org/10.1021/acs.est.5b04996.
462 Marsac, R., Martin, S., Boily, J.-F., Hanna, K., 2016. Oxolinic Acid Binding at Goethite and
463 Akaganéite Surfaces: Experimental Study and Modeling. Environ. Sci. Technol. 50, 660–668.
464 https://doi.org/10.1021/acs.est.5b04940.
465 Martínez-Mejía, M.J., Sato, I., Rath, S., 2017. Sorption mechanism of enrofloxacin on humic acids
466 extracted from Brazilian soils. Environ. Sci. Pollut. Res. 24, 15995–16006.
467 https://doi.org/10.1007/s11356-017-9210-3.
468 McKnight, D.M., Bencala, K.E., Zellweger, G.W., Aiken, G.R., Feder, G.L., Thorn, K.A., 1992.
469 Sorption of dissolved organic carbon by hydrous aluminum and iron oxides occurring at the
470 confluence of Deer Creek with the Snake River, Summit County, Colorado. Environ. Sci. Technol.
471 26, 1388–1396. https://doi.org/10.1021/es00031a017.
472 Oliphant, C.M., Green, G.M., 2002. Quinolones: a comprehensive review. Am. Fam. Physician 65,
473 455–464.

474 Peng, H., Liang, N., Li, H., Chen, F., Zhang, D., Pan, B., Xing, B., 2015. Contribution of coated
475 humic acids calculated through their surface coverage on nano iron oxides for ofloxacin and
476 norfloxacin sorption. Environ. Pollut. 204, 191–198.
477 https://doi.org/10.1016/j.envpol.2015.04.029.
478 Peuravuori, J., Pihlaja, K., 1997. Molecular size distribution and spectroscopic properties of aquatic
479 humic substances. Anal. Chim. Acta 337, 133–149.
480 https://doi.org/10.1016/S0003-2670(96)00412-6.
481 Qin, X., Du, P., Chen, J., Liu, F., Wang, G., Weng, L., 2018. Effects of natural organic matter with
482 different properties on levofloxacin adsorption to goethite: Experiments and modeling. Chem.
483 Eng. J. 345, 425–431. https://doi.org/10.1016/j.cej.2018.03.125.
484 Qin, X., Liu, F., Wang, G., 2012. Fractionation and kinetic processes of humic acid upon adsorption on
485 colloidal hematite in aqueous solution with phosphate. Chem. Eng. J. 209, 458–463.
486 https://doi.org/10.1016/j.cej.2012.08.026.
487 Qin, X., Liu, F., Wang, G., Hou, H., Li, F., Weng, L., 2015. Fractionation of humic acid upon
488 adsorption to goethite: Batch and column studies. Chem. Eng. J. 269, 272–278.
489 https://doi.org/10.1016/j.cej.2015.01.124.
490 Richter, M.K., Sander, M., Krauss, M., Christl, I., Dahinden, M.G., Schneider, M.K., Schwarzenbach,
491 R.P., 2009. Cation Binding of Antimicrobial Sulfathiazole to Leonardite Humic Acid. Environ.
492 Sci. Technol. 43, 6632–6638. https://doi.org/10.1021/es900946u.
493 Scheidegger, A., Borkovec, M., Sticher, H., 1993. Coating of silica sand with goethite: preparation and
494 analytical identification. Geoderma 58, 43–65. https://doi.org/10.1016/0016-7061(93)90084-X.

Seders Dietrich, L.A., McInnis, D.P., Bolster, D., Maurice, P.A., 2013. Effect of polydispersity on natural organic matter transport. Water Res. 47, 2231–2240. https://doi.org/10.1016/j.watres.2013.01.053.

Stumm, W., Sigg, L., Sulzberger, B., 1992. Chemistry of the solid-water interface: processes at the mineral-water and particle-water interface in natural systems. Wiley, New York.

Thorn, K.A., Cox, L.G., 2009. N-15 NMR spectra of naturally abundant nitrogen in soil and aquatic natural organic matter samples of the International Humic Substances Society. Org. Geochem. 40, 484–499. https://doi.org/10.1016/j.orggeochem.2009.01.007.

Valencia, S., Marín, J.M., Restrepo, G., Frimmel, F.H., 2013. Application of excitation–emission fluorescence matrices and UV/Vis absorption to monitoring the photocatalytic degradation of commercial humic acid. Sci. Total Environ. 442, 207–214. https://doi.org/10.1016/j.scitotenv.2012.10.058.

van Genuchten, M.Th., Wagenet, R.J., 1989. Two-Site/Two-Region Models for Pesticide Transport and Degradation: Theoretical Development and Analytical Solutions. Soil Sci. Soc. Am. J. 53, 1303. https://doi.org/10.2136/sssaj1989.03615995005300050001x.

Vindedahl, A.M., Stemig, M.S., Arnold, W.A., Penn, R.L., 2016. Character of Humic Substances as a Predictor for Goethite Nanoparticle Reactivity and Aggregation. Environ. Sci. Technol. 50, 1200–1208. https://doi.org/10.1021/acs.est.5b04136.

Weng, L., Van Riemsdijk, W.H., Hiemstra, T., 2007. Adsorption of humic acids onto goethite: Effects of molar mass, pH and ionic strength. J. Colloid Interface Sci. 314, 107–118. https://doi.org/10.1016/j.jcis.2007.05.039.

516 Xu, J., Marsac, R., Costa, D., Cheng, W., Wu, F., Boily, J.-F., Hanna, K., 2017a. Co-Binding of
517 Pharmaceutical Compounds at Mineral Surfaces: Molecular Investigations of Dimer Formation at
518 Goethite/Water Interfaces. Environ. Sci. Technol. 51, 8343–8349.
519 https://doi.org/10.1021/acs.est.7b02835.
520 Xu, J., Marsac, R., Wei, C., Wu, F., Boily, J.-F., Hanna, K., 2017b. Cobinding of Pharmaceutical
521 Compounds at Mineral Surfaces: Mechanistic Modeling of Binding and Cobinding of Nalidixic
522 Acid and Niflumic Acid at Goethite Surfaces. Environ. Sci. Technol. 51, 11617–11624.
523 https://doi.org/10.1021/acs.est.7b02900.
524 Yan, W., Hu, S., Jing, C., 2012. Enrofloxacin sorption on smectite clays: Effects of pH, cations, and
525 humic acid. J. Colloid Interface Sci. 372, 141–147. https://doi.org/10.1016/j.jcis.2012.01.016.
526 Yu, C., Bahashi, J., Bi, E., 2019. Mechanisms and quantification of adsorption of three
527 anti-inflammatory pharmaceuticals onto goethite with/without surface-bound organic acids.
528 Chemosphere 222, 593–602. https://doi.org/10.1016/j.chemosphere.2019.01.155.
529 Zhou, Q., Maurice, P.A., Cabaniss, S.E., 2001. Size fractionation upon adsorption of fulvic acid on
530 goethite: equilibrium and kinetic studies. Geochim. Cosmochim. Acta 65, 803–812.
531 https://doi.org/10.1016/S0016-7037(00)00536-6.

Highlights

- NOM compounds with higher aromaticity and lower Mw are preferentially adsorbed.
- NOM fractionation alters sorption mechanisms and kinetics of quinolones.
- Multiple mechanisms influence NA mobility when NOM are present together with NA.
- Nonspecific interactions govern NA mobility when NOM are found as mineral coatings.
- A transport model is developed to interpret the modifications in binding mechanisms.

Credit Author Statement:

WC, RM and KH designed the study. WC carried out the experiments and wrote the manuscript. LZ performed the calculations**.** JFB and KH: Wrote, reviewed and edited the manuscript. All authors discussed the results and commented on the manuscript.

Declaration of interests

☒ The authors declare that they have no known competing financial interests or personal relationships that could have appeared to influence the work reported in this paper.

☐The authors declare the following financial interests/personal relationships which may be considered as potential competing interests: